pound Al_2Ru which is orthorhombic and has comparable strength of atomic potential to the *i*-phases, does have a real gap. It is mentioned above that electrons in a quasiperiodic lattice are prone to localization [also see (*26*)], and the extent of the effect depends on the form of the atomic potential in an alloy. Meanwhile, whether the absence of a real gap is also due to "quasiperiodicity" needs to be investigated. Taking a different viewpoint, an internal structural model (*27*) advocates that in the ordered *i*-phases, the icosahedral atomic blocks that are metallic, are enveloped by a layered-structure network that is insulating with an energy gap. This structural arrangement leads to a proximity tunneling type of conductivity with a finite density of states at the Fermi level. Clearly, much research is needed for understanding electron localization and band-gap formation in metallic quasicrystals as well as ordered metallic systems in general.

REFERENCES AND NOTES

1. D. Shechtman *et al.*, *Phys. Rev. Lett.* **53**, 1951 (1984).
2. D. Levine and P. J. Steinhardt, *ibid.*, p. 2477.
3. D. P. DiVincenzo and P. J. Steinhardt, Eds., *Quasicrystals: The State of the Art, Directions in Condensed Matter Physics, vol. 11* (World Scientific, Singapore, 1991).
4. P. W. Stephens and A. I. Goldman, *Sci. Am.* **264**, 44 (April 1991); A. I. Goldman and M. Widom, *Annu. Rev. Phys. Chem.* **42**, 685 (1991). These provide tutorials on the indexing of icosahedral crystals.
5. T. Fujiwara and H. Tsunetsugu, in (*3*), p. 343.
6. H. Hiramoto and M. Kohmoto, *Int. J. Mod. Phys. B* **6**, 281 (1992).
7. L. S. Levitov, *Europhys. Lett.* **7**, 343 (1988); M. Kohmoto and H. Hiramoto, *Int. J. Mod. Phys. B*, in press. As in (*5*) the models are one- and two-dimensional. However, it was speculated that the key features noted could be extrapolated to three dimensions.
8. K. Kimura and S. Takeuchi, in (*3*), p. 313.
9. S. J. Poon, *Adv. Phys.* **41**, 303 (1992).
10. P. A. Lee and T. V. Ramakrishnan, *Rev. Mod. Phys.* **57**, 287 (1985); also articles in *Electron-Electron Interactions in Disordered Systems*, edited by A. L. Efros and M. Pollak (North-Holland, Amsterdam, 1985). It should be pointed out that there is a class of cerium and uranium metallic compounds known as Kondo insulators that exhibit semiconducting behavior, apparently ascribable to the formation of a spin gap. See for example, G. Aeppli and Z. Fisk, *Comm. Condens. Matter Phys.* **16**, 155 (1992).
11. P. A. Heiney *et al.*, *Science* **238**, 660 (1987).
12. For a review, see A. P. Tsai *et al.*, in *Physics and Chemistry of Finite Systems: From Clusters to Crystals*, NATO ASI Series, P. Jena, S. N. Khanna, and B. K. Rao, Eds. (Kluwer, Boston, 1992), vol. I, p. 39.
13. C. Guryan *et al.*, *Phys. Rev. Lett.* **62**, 2409 (1989); P. Bancel, *ibid.* **63**, 2741 (1989); A. R. Kortan *et al.*, *ibid.* **64**, 200 (1990).
14. AlCuRu, ~30,000 μohm-cm, $R \sim 4$. [B. D. Biggs, S. J. Poon, N. R. Munirathnam, *ibid.* **65**, 2700 (1990).]
15. AlCuFe, ~10,000 μohm-cm, $R \sim 2.3$. [T. Klein *et al.*, *ibid.* **66**, 2907 (1991); also T. Klein *et al.*, *Europhys. Lett.* **13**, 129 (1990).]
16. AlPdMn, ~ 9,500 μohm-cm, $R \sim 2$. [P. Lanco *et al.*, *Europhys. Lett.* **18**, 227 (1992).]
17. AlPdRe, ~120,000 μohm-cm, $R \sim 10$. (K. Edagawa *et al.*, unpublished results.)
18. C. C. Homes *et al.*, *Phys. Rev. Lett.* **67**, 2694 (1991).
19. A. E. Carlsson, *Nature* **353**, 15 (1991); *Phys. Rev. B* **47**, 2515 (1993).
20. J. L. Wagner *et al.*, *Phys. Rev. B* **38**, 7436 (1988); B. D. Biggs, thesis, University of Virginia (1992).
21. N. F. Mott, *Conduction in Non-Crystalline Materials* (Oxford Univ. Press, New York, 1987). The conduction models include those based on the variable range hopping and scaling theories.
22. A. P. Smith and N. W. Ashcroft, *Phys. Rev. Lett.* **59**, 1365 (1987); V. G. Vaks, V. V. Kamyshenko, G. D. Samolyuk, *Phys. Lett. A* **132**, 131 (1988); J. Freidel, *Helv. Phys. Acta* **61**, 538 (1988).
23. A. Sadoc *et al.*, *J. Non-Cryst. Solids* **153 & 154**, 338 (1993); E. Belin, in (*12*), p. 829.
24. F. S. Pierce and S. J. Poon, unpublished results. In view of the fact that the states near the Fermi level are localized, the rapid rise in conductivity above ~400°K is determined by the activation of these states into the conduction band. Since the Fermi level is located near the top of the valence band, the use of $\rho \propto e^{E_g/k_BT}$ is appropriate.
25. D. N. Manh *et al.*, *Solid State Commun.* **82**, 329 (1992).
26. A. Yu. Kitaev, *Sov. Phys.–JETP Lett.* **48**, 298 (1990).
27. J. C. Phillips and K. M. Rabe, *Phys. Rev. Lett.* **66**, 923 (1991).
28. This work was supported by National Science Foundation contract DMR90-15538.

9 April 1993; accepted 11 June 1993

Thorium-Uranium Fractionation by Garnet: Evidence for a Deep Source and Rapid Rise of Oceanic Basalts

T. Z. LaTourrette,* A. K. Kennedy,† G. J. Wasserburg

Mid-ocean ridge basalts (MORBs) and ocean island basalts (OIBs) are derived by partial melting of the upper mantle and are marked by systematic excesses of thorium-230 activity relative to the activity of its parent, uranium-238. Experimental measurements of the distribution of thorium and uranium between the melt and solid residue show that, of the major phases in the upper mantle, only garnet will retain uranium over thorium. This sense of fractionation, which is opposite to that caused by clinopyroxene-melt partitioning, is consistent with the thorium-230 excesses observed in young oceanic basalts. Thus, both MORBs and OIBs must begin partial melting in the garnet stability field or below about 70 kilometers. A calculation shows that the thorium-230–uranium-238 disequilibrium in MORBs can be attributed to dynamic partial melting beginning at 80 kilometers with a melt porosity of 0.2 percent or more. This result requires that melting beneath ridges occurs in a wide region and that the magma rises to the surface at a velocity of at least 0.9 meter per year.

Information about the rate at which a source region melts and the magma is transported to the surface of the Earth can provide key constraints on magmatic plumbing systems in the mantle and crust. One important source of this information is isotopic disequilibrium among the members of the uranium-series decay chain in young oceanic basalts. Most young MORBs and OIBs display secular disequilibrium between ^{230}Th and ^{238}U, with the activity of ^{230}Th enriched relative to that of ^{238}U (*1*). This disequilibrium implies that the basalts have a higher Th/U ratio than the mantle from which they were derived. Such a Th-U fractionation generates a transient excess of ^{230}Th relative to its parent, ^{238}U, in the basalt. Because a system will return to secular equilibrium (where the ^{230}Th and ^{238}U activities are equal) within about five half-lives of ^{230}Th (or 377,000 years), ^{230}Th-^{238}U disequilibrium reflects recent chemical fractionation of Th from U and can be used to constrain the timing of magma generation and transport. In order to interpret this disequilibrium, however, the origin of the Th-U fractionation, that is, the location and the time in the erupted lava's history when the fractionation occurred, must be determined.

Many workers have attributed the Th-U fractionation to differences in crystal-melt partitioning between Th and U during partial melting (*1–3*). Recent experimental trace-element partitioning studies have shown that partial melting of spinel lherzolite is not a possible explanation of ^{230}Th-^{238}U disequilibrium in young oceanic basalts, as a partial melt from such a source will be enriched in U relative to Th, which is opposite to what is found (*4, 5*). This conflict could be resolved if partial melting occurred at higher pressures where other phases controlled the Th and U partitioning. We thus conducted partitioning experiments between garnet and melt to evaluate the possibility that ^{230}Th-^{238}U disequilibri-

---

Division of Geological and Planetary Sciences, California Institute of Technology, Pasadena, CA 91125.

*To whom correspondence should be addressed at Department of Geology, Box 1404, Arizona State University, Tempe, AZ 85287.

†Present address: Department of Applied Physics, Curtin University of Technology, Perth, 6001, Australia.

um in young oceanic basalts results from partial melting of garnet lherzolite.

Garnet crystals were grown from a mixture of oxides at 27 kbar in a 0.5-inch piston-cylinder press with CaF_2 pressure cells and crushable MgO spacers. Crystals were grown by the slow cooling of the sample from the liquidus temperature (1355°C) (*4, 6*). After it was pressurized, the sample was brought to the liquidus temperature and held for 30 min and then was cooled at a rate of 4° to 6°C per hour; we quenched the samples at selected temperatures by shutting off the power to the furnace. Uranium is multivalent, and its crystal-melt partitioning behavior is sensitive to the fugacity of oxygen, fO_2 (*4*). By using graphite capsules sealed in platinum, we constrained the fO_2 of the experiments to be below that of the graphite-CO-CO_2 oxygen buffer (*7*). For these experimental conditions this buffer gives $\log fO_2 = -7.20$ (*8*), which is in accord with values inferred for MORBs (*9*).

Crystals and glass were analyzed for major elements with an electron microprobe, and Th, U, and Sm were measured with PANURGE, a modified Cameca ims-3f secondary ion mass spectrometer (SIMS) (*10*). Ion intensities normalized to ^{30}Si were converted to concentrations by means of a sensitivity factor determined from a standard. As no suitable Th or U standards were available for garnet, we calculated concentrations by assuming that the ratio of sensitivity factors for Th and U between garnet and glass were the same as for Sm (1.15).

The experiments yielded a small number of medium to large (40 to 70 μm in diameter) euhedral garnet crystals plus numerous smaller (5 to 25 μm) garnet crystals and quenched silicate melt. The concentrations of Th and U in the glass are uniform within measurement error (Table 1), indicating that these elements remained homogeneous in the melt during crystal growth. As expected in slow cooling experiments, the crystals were chemically zoned in response to changing melt composition, although the fractions of melt crystallized (Table 1) were purposely kept small to minimize zoning. The extent of zoning (in terms of the pyrope, almandine, and grossular components), ranged from $Py_{48}Al_{38}Gr_{14}$ to $Py_{39}Al_{42}Gr_{19}$.

Partition coefficients (Table 2) for all crystals analyzed are consistent: the intercrystal standard deviation is less than the errors in the counting statistics. The Sm partition coefficients (Table 2) compare well with those from earlier experimental measurements of similar composition (*11*). Most SIMS analyses were confined to the cores of the crystals. One crystal rim analysis was obtained and gave a slightly higher apparent partition coefficients than those for the core, consistent with increasing incompatible element concentrations from core to rim. Because the crystal fraction is small, correction for this zoning (*4*) has been neglected, as this correction is small compared to the analytical error.

The data show that garnet retains U over Th by nearly an order of magnitude (Table 2); as a result, Th is enriched relative to U in the extracted melt. This observation demonstrates that the sense of Th-U fractionation by garnet-melt partitioning is opposite to that in clinopyroxene (*4, 5*), consistent with other recent results (*12*). A melt coexisting with garnet will have a Th/U ratio much larger than that of the garnet in the residual solid (Fig. 1). This sense of Th-U fractionation is consistent with the ^{230}Th excesses found in young oceanic basalts and strongly suggests that the ^{230}Th-^{238}U disequilibrium in these lavas results from Th-U fractionation by residual garnet during partial melting.

These partition coefficients can be used in a single-stage batch melting model of a garnet-bearing lherzolite to generate a ^{230}Th activity excess in the extracted melt. However, in order to produce the degree of ^{230}Th excess observed in oceanic basalts, this model requires that a small total degree of melting (<0.2%) occur entirely in the garnet stability field, which is not very realistic. Slow melting of upwelling mantle with continuous withdrawal of melt is more likely.

To explore this latter scenario, we calculated the degree of ^{230}Th-^{238}U disequilibrium produced during dynamic partial melting (*2*), which approximates pressure-release melting of a column of upwelling mantle beneath a mid-ocean ridge. A key factor in this model is that melting be slow enough for the ^{230}Th and ^{238}U remaining in the mantle to stay in secular equilibrium. The ^{230}Th that is extracted by melting is thus effectively replaced in the mantle by radioactive decay of ^{238}U. In this way, ^{230}Th excesses can be sustained for large degrees of partial melting. The results (Fig. 2) indicate that ^{230}Th-^{238}U disequilibrium in MORBs can be attributed to dynamic partial melting beginning at a depth of 80 km. Although only 14% of the melting occurs in the garnet stability field, the bulk of the Th and U are extracted from the upwelling mantle in the early stages of melting. Hence, the ^{230}Th-^{238}U disequilibrium signature is dominated by melt generated from garnet lherzolite. The ^{230}Th excess in most samples can be accommodated by melt porosities of 0.2% or more (Fig. 2). The greater ^{230}Th excesses in a few samples may be the result of lower total melt fractions, anomalously slow melting, very low melt porosity, or the addition of Th (or removal of U) by some process

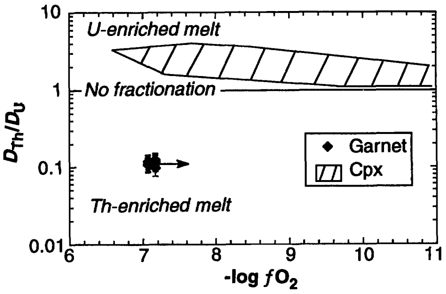

Fig. 1. Ratio of garnet-melt partition coefficients for Th and U (D_{Th}/D_U) plotted against oxygen fugacity. Horizontal arrow on the points indicates that the fO_2 plotted is for the graphite-CO-CO_2 buffer and is an upper limit for the actual conditions of the experiments. Results from clinopyroxene partitioning experiments for natural MORB composition (*4*) are shown for reference. The value of D_{Th}/D_U is less than 1 for garnet, in contrast to clinopyroxene, indicating that residual garnet will preferentially retain U over Th during partial melting and thus that a partial melt will have a Th/U ratio greater than that of its source.

Table 1. Compositions of the starting material and run products. The oxide compositions are in percent by weight. Concentrations of Th, U, and Sm are in parts per million.

Component	Starting composition*	Run 6		Run 8	
		Garnet	Glass	Garnet	Glass
SiO_2	60.7	40.0	63.3	38.5	64.4
TiO_2	1.05	1.13	1.14	0.66	1.02
Al_2O_3	16.8	22.6	16.5	22.9	17.5
FeO*†	5.82	19.6	4.92	19.4	4.93
MgO	2.39	11.7	1.55	11.9	1.42
CaO	4.95	5.9	5.03	6.02	4.92
Na_2O	3.16	0.05	2.99	0.06	3.43
K_2O	2.00		2.16		2.19
Th	8200 ± 400	14 ± 2	8200 ± 1100	16 ± 3	9300 ± 1300
U	7900 ± 500	118 ± 13	8000 ± 1100	126 ± 20	8300 ± 1300
Sm	3300 ± 400	1010 ± 101	2150 ± 100	1160 ± 120	2350 ± 100
Total	98.6	101.1	99.8	99.4	99.8

Analysis of super liquidus quench glass. †FeO = total Fe as FeO.

other than partial melting.

Although these results provide a probable explanation for the ^{230}Th excess in oceanic basalts, Th-U fractionation by some accessory phase such as apatite could also be important. There is no evidence for the presence of apatite in the oceanic mantle, however, and the ubiquity of ^{238}U-^{230}Th disequilibrium in oceanic basalts thus suggests that the behaviors of Th and U are controlled by primary phases. In addition, accessory phases such as apatite have high solubilities in basalts (*13*) and would probably be consumed during melting, leaving no fractionation signature.

Our conclusion that ^{230}Th-^{238}U disequilibrium in young MORBs results from partial melting of garnet lherzolite is consistent with other evidence for the presence of garnet in the MORB source, including Lu-Hf isotopes (*14*) and rare earth element distributions in MORBs (*15, 17*) and abyssal peridotites (*18*). In the present model the La/Yb ratio of the melt is enriched by a factor of 1.4 relative to the source, in agreement with the results of Langmuir *et al.* (*15*). This model also generates the correct sense of Lu-Hf fractionation required to explain the low ^{176}Lu/^{177}Hf in MORBs, although, in contrast to the ^{238}U-^{230}Th disequilibrium data, the depth at which melting must begin to account for most of the Lu-Hf data [>300 km (*14*)] may be unrealistically high. The reason for this discrepancy is unknown.

In order to produce large degrees of ^{230}Th-^{238}U disequilibrium, the melting rate of the rising mantle must be quite low, which requires that the mantle upwelling rate be less than the half-spreading rate at most ridges. This, in turn, requires that melting occur in a region much wider than the narrow active volcanic zone observed at mid-ocean ridges. This result supports the conclusions of McKenzie (*19*) that melting is slow, melt porosities are low, and melting occurs over a wide region beneath mid-ocean ridges. These results also allow us to estimate magma transit rates at mid-ocean ridges. In order to preserve its disequilibrium signature, the magma must reach the surface before the ^{230}Th excess decays significantly. Most of the ^{230}Th-^{238}U disequilibrium is generated in the garnet stability field near the base of the melting region and therefore must travel from below the spinel-garnet transition to the surface within about one ^{230}Th half-life (75,400 years). For a transition depth of 70 km the magma must travel at least 0.9 m/year. For these low melt fractions to percolate so far so quickly, their viscosities must be quite low, possibly requiring high CO_2 contents. This implies that oceanic basalts might contain a carbonatitic component, although no evidence for this has been found.

These results can also be applied to ^{230}Th-^{238}U disequilibrium in OIBs. Evidence from rare-earth element, major element, and geophysical data show that OIBs form from melting that begins in the garnet stability field and that garnet remains in the residuum (*20, 21*). It is therefore highly likely that the ^{230}Th excesses in OIBs also result from Th-U fractionation by residual garnet. Genesis of alkali basalt, a common type of OIB magma, requires a higher mean melting pressure and hence a higher fraction of the melting in the presence of garnet than that of MORB (*21*). From this distinction one would expect that the average ^{230}Th excess in OIBs be higher than that in MORBs, which is exactly what has been found (*22*).

In addition to the partition coefficients, the details of the chosen melting model will affect the predicted degree of ^{230}Th enrichment. For example, recent modeling by Spiegelman and Elliott (*23*) takes into account the effects of melt transport through the matrix in generating ^{230}Th-^{238}U disequilibrium. This model may better simulate the conditions of magma generation in the mantle and hence further refine the melting and magma transit rates derived in this work. In addition, phase compositions can be significantly different in systems that contain both garnet and clinopyroxene (*24*). These changes may affect trace-element partition coefficients and hence the relative degree to which clinopyroxene and garnet contribute to Th-U fractionation. In any case, the fact that residual garnet will retain U over Th by nearly an order of magnitude is strong evidence that garnet plays a key role in Th-U fractionation in the genesis of oceanic basalts.

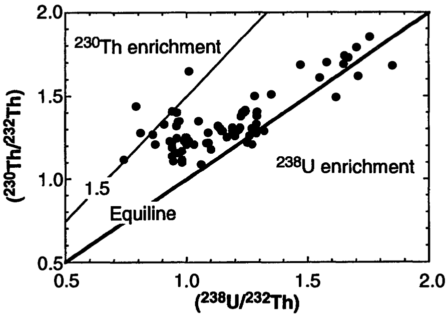

Fig. 2. A ^{230}Th-^{238}U disequilibrium diagram showing data for MORBs (*3, 25*) and calculated ^{230}Th-^{238}U disequilibrium generated for dynamic partial melting (*2*) of an upwelling mantle. Parentheses indicate activities. Samples in secular equilibrium have (^{230}Th/^{232}Th) = (^{238}U/^{232}Th) and thus lie on the one-to-one equiline. Th-U fractionation will move a sample off the equiline, and essentially all MORBs plot to the left, indicating ^{230}Th enrichment within the last 375,000 years. The curve labeled 1.5 delineates the calculated locus of points corresponding to ^{230}Th excess of 50%, that is, (^{230}Th/^{232}Th) = 1.5 (^{238}U/^{232}Th), generated by partial melting with the following parameters: melting begins at 80 km and ends at 10 km, upwelling rate is 1 cm/year, total melt fraction extracted equals 0.13, melt porosity (the melt fraction beyond which melt is instantaneously extracted) increases linearly from 0 at the base of the melting region to 0.4% at the top (*23*) (average porosity = 0.2%), the source consists of olivine + orthopyroxene + clinopyroxene + either spinel or garnet, the transition from garnet to spinel lherzolite is at 70 km, partition coefficients are from this study (Table 2) and (*5, 26*), and phase proportions are from (*17*). In a given parcel of mantle the ^{238}U and ^{230}Th concentrations decrease rapidly at the onset of melting, and therefore the ^{230}Th-^{238}U disequilibrium signature is dominated by the melt formed in the garnet stability field.

Table 2. Partition coefficients of the run products.

Parameter	Run 6	Run 8
F_{xtl}*	0.10	0.14
$D_{Th}^{garnet/melt}$†	0.0017 ± 0.0003	0.0017 ± 0.0004
$D_{U}^{garnet/melt}$	0.015 ± 0.003	0.015 ± 0.003
D_{Th}/D_{U}	0.11 ± 0.03	0.11 ± 0.04
$D_{Sm}^{garnet/melt}$	0.47 ± 0.05	0.49 ± 0.06

*F_{xtl} = crystal fraction. Runs 6 and 8 were quenched at 1313° and 1307°C, respectively. †$D_i^{garnet/melt}$ = C_i^{garnet}/C_i^{melt}, where C is concentration. The Th, U, and Sm partition coefficients are averages of four crystals in each sample.

REFERENCES AND NOTES

1. J. B. Gill, D. M. Pyle, R. W. Williams, in *Uranium Series Disequilibrium: Applications to Environmental Problems*, M. Ivanovitch and R. S. Harmon, Eds. (Oxford Univ. Press, New York, ed. 2, 1992), pp. 207–258; M. Condomines, Ch. Hemond, C. J. Allègre, *Earth Planet. Sci. Lett.* **90**, 243 (1988).
2. R. W. Williams and J. B. Gill, *Geochim. Cosmochim. Acta* **53**, 1607 (1989).
3. D. Ben Othman and C. J. Allègre, *Earth Planet. Sci. Lett.* **98**, 129 (1990); S. J. Goldstein, M. T. Murrell, D. R. Janecky, J. R. Delaney, D. A. Clague, *ibid.* **109**, 255 (1992).
4. T. Z. LaTourrette and D. S. Burnett, *ibid.* **110**, 227 (1992).
5. P. Beattie, *Eos* **73**, 616 (1992).
6. This method was chosen because steep chemical zoning profiles in garnet crystals grown isothermally at 1325°C indicate a failure to attain equilibrium after 72 hours.
7. J. R. Holloway, V. Pan, G. Gudmunsson, *Eur. J. Mineral.* **4**, 105 (1992).
8. P. Ulmer and R. W. Luth, *Contrib. Mineral. Petrol.* **106**, 265 (1991).
9. D. M. Christie, I. S. E. Carmichael, C. H. Langmuir, *Earth Planet. Sci. Lett.* **79**, 397 (1986).

10. A 1-nA primary beam of O⁻ ions was focused to give a spot size of approximately 10 μm. An offset voltage of −45 V suppressed undesirable molecular ion interferences [E. Zinner and G. Crozaz, *Int. J. Mass Spectrom. Ion Processes* **69**, 17 (1986)].
11. I. A. Nicholls and K. L. Harris, *Geochim. Cosmochim. Acta* **44**, 287 (1980).
12. P. Beattie, *Nature* **363**, 63 (1993).
13. E. B. Watson, *Earth Planet. Sci. Lett.* **51**, 322 (1980).
14. V. J. M. Salters and S. R. Hart, *Nature* **342**, 420 (1989).
15. C. H. Langmuir, J. F. Bender, A. E. Bence, G. N. Hansen, S. R. Taylor, *Earth Planet. Sci. Lett.* **36**, 133 (1977).
16. J. F. Bender, C. H. Langmuir, G. N. Hansen, *J. Petrol.* **25**, 213 (1984).
17. D. McKenzie and R. K. O'Nions, *ibid.* **32**, 1021 (1991).
18. K. T. M. Johnson, H. J. B. Dick, N. Shimizu, *J. Geophys. Res.* **95**, 2661 (1990).
19. D. McKenzie, *Earth Planet. Sci. Lett.* **72**, 149 (1985).
20. F. A. Frey *et al.*, *J. Geophys. Res.* **96**, 14347 (1991); R. W. Kay and P. W. Gast, *J. Geol.* **81**, 653 (1973); S. Watson and D. McKenzie, *J. Petrol.* **32**, 501 (1991).
21. H. S. Yoder and C. E. Tilly, *J. Petrol.* **3**, 342 (1962).
22. J. Gill and M. Condomines, *Science* **257**, 1368 (1992).
23. M. Spiegelman and T. Elliott, in preparation.
24. For example, clinopyroxene coexisting with garnet can have considerably less Al than clinopyroxene in garnet-free systems [G. P. Brey, T. Köhler, K. G. Nickel, *J. Petrol.* **31**, 1313 (1990)].
25. M. Condomines, P. Morand, C. J. Allègre, *Earth Planet. Sci. Lett.* **55**, 247 (1981); S. J. Goldstein, M. T. Murrell, D. R. Janecky, *ibid.* **96**, 134 (1989); S. Krishnaswami, K. K. Turekian, J. T. Bennett, *Geochim. Cosmochim. Acta* **48**, 505 (1984); S. Newman, R. C. Finkel, J. D. Macdougall, *Earth Planet. Sci. Lett.* **65**, 17 (1983); I. Reinitz and K. K. Turekian, *ibid.* **94**, 199 (1989); K. H. Rubin and J. D. Macdougall, *Nature* **335**, 158 (1988).
26. T. LaTourrette, thesis, California Institute of Technology (1992); A. K. Kennedy, G. E. Lofgren, G. J. Wasserburg, *Earth Planet. Sci. Lett.* **115**, 177 (1993). Clinopyroxene partition coefficients from (*5*) were used because they are from high-pressure experiments and thus may more realistically represent natural conditions than those of (*4*); partition coefficients for spinel are assumed to be 0.

27. We thank M. Baker and I. Hutcheon for assistance in the laboratory and D. Burnett, E. Stolper, M. Spiegelman, and P. Beattie for helpful discussions. This work was supported by a fellowship from the National Aeronautics and Space Administration (NASA) Graduate Student Researchers Program (T.Z.L.) and NASA grant NAGW-3297 (G.J.W.). Division contribution 5253 (805).

18 March 1993; accepted 2 June 1993

Ices on the Surface of Triton

Dale P. Cruikshank, Ted L. Roush, Tobias C. Owen,
Thomas R. Geballe, Catherine de Bergh, Bernard Schmitt,
Robert H. Brown, Mary Jane Bartholomew

The near-infrared spectrum of Triton reveals ices of nitrogen, methane, carbon monoxide, and carbon dioxide, of which nitrogen is the dominant component. Carbon dioxide ice may be spatially segregated from the other more volatile ices, covering about 10 percent of Triton's surface. The absence of ices of other hydrocarbons and nitriles challenges existing models of methane and nitrogen photochemistry on Triton.

Voyager 2 revealed Triton as a frozen world with a relatively young and highly structured surface almost devoid of impact craters and with evidence of episodes of local and perhaps global melting (*1*). A tenuous atmosphere of nitrogen and methane supports a tropospheric photochemical haze layer, discrete clouds, and winds that blow the effluent from at least three active plumes (or "geysers") toward the equator from the south polar region (*2*). Solid N_2 and CH_4 had been detected on Triton's surface by earlier ground-based telescopic observations (*3*, *4*). The atmospheric pressure of 16 ± 3 microbar N_2 was found to be in approximate vapor pressure equilibrium with the surface ice.

We have continued to observe Triton with ground-based telescopes to probe further details of its composition. In this report we describe the results of our 1991 and 1992 investigations of the reflectance spectrum of Triton obtained with a new infrared spectrometer at the 3.8-m United Kingdom Infrared Telescope Facility on Mauna Kea, Hawaii (*5*).

Our spectra have significantly higher (250–350) resolving power and signal-to-noise than had been previously achieved. We confirm the presence of the six bands of CH_4 and one band of N_2 that had been seen in the earlier data, but obtain more precise measurements of the band strengths, shapes, and central wavelengths. The spectra also show absorption bands due to solid CO and CO_2.

Seen from Earth, Triton is unresolved (subtended diameter <0.2 arc sec), and the telescopic spectra reported here result from sunlight reflected from an entire hemisphere. Reflection from the icy surface of Triton occurs by scattering from individual grains and depends on the grain diameters and refractive indices of the various ice components. Near-infrared spectroscopy probes the uppermost several centimeters of the surface.

In Hapke's (*6*) model of scattering from a particulate surface, from the real (*n*) and imaginary (*k*) indices of refraction of a material one can calculate the reflectance of both multi- and monocomponent surfaces (*7*). We have used this theory to calculate the radiance factor, which is the reflectance of Triton's surface relative to that of a perfect reflecting lambert surface illuminated and viewed normally, using three different models of the surface ices. The first (checkerboard) model has spatially segregated patches of the four identified ices, and a single solar photon is scattered from a grain of only one kind of ice. The second (salt-and-pepper) model consists of intimate mixtures of ices, in which a photon may be multiply scattered from grains of different composition. In the third kind of model, ices are mixed at the molecular level (for example, CH_4 dissolved in N_2 in a solid solution). We used the optical constants of the pure ices (*8*) in the spatially segregated and intimate mixture models, and additional data (*9*) for models of molecular mixtures of CH_4 and N_2. Laboratory data on the molecular mixes are not yet adequate for our models, and the results reported here pertain only to intimate mixes and spatially segregated components.

With four molecular species identified on Triton's surface, and with the possibilities of spatially segregated pure and mixed ices in various particle sizes, a model fit to the observed spectrum involves many parameters, which are therefore difficult to constrain. In general, larger particles and greater fractional coverage of the surface generate stronger absorption bands, while smaller particles of any constituent will yield weaker bands of all the constituents. In a model fit to the spectrum the behaviors of absorption bands of the four constituents are interrelated, but we first consider each of the components separately.

Molecular nitrogen is the most volatile constituent identified, and gaseous N_2 dominates the atmosphere. Sublimation and condensation of N_2 appear to maintain an

---

D. P. Cruikshank, NASA Ames Research Center, MS 245-6, Moffett Field, CA 94035–1000.
T. L. Roush, Department of Geosciences, San Francisco State University, San Francisco, CA 94132, and NASA Ames Research Center, MS 245-3, Moffett Field, CA 94035–1000.
T. C. Owen, Institute for Astronomy, University of Hawaii, 2680 Woodlawn Drive, Honolulu, HI 96822.
T. R. Geballe, Joint Astronomy Center, 660 North Aohoku Place, University Park, Hilo, HI 96720.
C. de Bergh, Observatoire de Paris, 5 Place Jules Janssen, 92195 Meudon Cedex, France.
B. Schmitt, Laboratoire de Glaciologie et Geophysique de l'Environnement, BP 96, 38402 Saint-Martin d'Heres, France.
R. H. Brown, Jet Propulsion Laboratory, MS 183-501, 4800 Oak Grove Drive, Pasadena, CA 91109.
M. J. Bartholomew, Sterling Software Inc., 1121 San Antonio Road, Palo Alto, CA 94303, and NASA Ames Research Center, MS 245-6, Moffett Field, CA 94035–1000.